Sputter roughening of inhomogeneous surfaces: Impurity pinning and nanostructure shape selection

S. W. Ong,[1] E. S. Tok,[2] and H. Chuan Kang[1,*]
[1]*Department of Chemistry, National University of Singapore, 10 Kent Ridge Crescent, Singapore*
[2]*Department of Physics, National University of Singapore, 10 Kent Ridge Crescent, Singapore*
(Received 8 May 2006; revised manuscript received 12 February 2007; published 28 June 2007)

A model is proposed for sputter roughening of inhomogeneous systems with slowly sputtered impurity particles randomly distributed in the bulk. Surface inhomogeneity, which develops as a result of coupling between the time evolution of the local surface impurity concentration and the local surface shape, is tuned by changing the dependence of the sputtering probability upon impurity concentration. In 1+1dimensions, we find long-time scaling exponents that are consistent with Kardar—Parisi—Zhang (KPZ) values. However, for a range of surface inhomogeneity, impurity pinning results in a persistent growth regime where the surface roughens rapidly. We correlate this rapid roughening to fluctuations of the impurity concentration at the surface. Roughening in this regime leads to the formation of cones whose shape is determined by material property and sputtering flux, suggesting a unique method of nanostructure fabrication. In 2+1 dimensions, a similar variation of the roughening behavior with surface inhomogeneity is observed. For small surface inhomogeneity, there is an initial exponential roughening followed by power-law roughening with an effective growth exponent much smaller than KPZ. For larger surface inhomogeneity two power-law roughening regimes are observed, with an initial rapid roughening that crosses over to slower roughening; the effective exponent in each of these regimes increases with surface inhomogeneity. The surface morphology observed in the simulations is considerably noisier than experimental data for InP and GaSb. Our model shows noisy nonlinear pattern formation in contrast to the marked long-range hexagonal ordering seen in experiments. However, the scaling behavior is robust enough that roughening kinetics similar to that observed experimentally can be obtained depending upon the values of inhomogeneity and the strength of the nonlinear term in the model.

DOI: 10.1103/PhysRevE.75.061607 PACS number(s): 68.03.Hj, 68.35.Fx, 68.49.Sf, 81.07.−b

There is considerable interest in the physics of sputtering because of its potential for applications in quantum devices and optoelectronics where fabricating nanostructures with reproducible and controllable shape and size is desirable. When an ion hits a surface the number of surface atoms sputtered depends on the curvature of the surface [1]. This dependence of the sputtering yield upon surface curvature leads to an exponentially roughening instability. Competition between this roughening instability and the smoothening effect due to surface diffusion determines the length and time scales of the growth dynamics of the nanostructures formed during sputtering. This basic understanding of sputter roughening has been refined by the inclusion of nonlinear effects and noise, leading to the use of the Kuramoto-Sivashinsky (KS) equation to describe the evolution of the topography of the surface [2–6].

Thus far, theoretical descriptions of sputter roughening have focused upon homogeneous surfaces where the sputter yield is dependent only upon the surface shape but not upon the identity of the surface atoms. On the other hand, sputter-roughening experiments have been reported for systems with more than one atomic species [7–12]. Even though the long-time roughening behavior in these systems can be reasonably understood using the KS equation, there appears to be an initial rapidly power-law roughening regime that is *not consistent* with the KS equation. Furthermore, the shape of the nanostructures formed is *lenticular* in single-species systems such as silicon [13,14], germanium [15], and iron [16], but *conical* in mixed systems such as InP [7] and GaSb [8]. Generally, mixed systems roughen significantly more rapidly than single-species systems, leading, to a much larger ratio of roughness to the number of sputtered layers [7–9,13,14]. For example, in otherwise similar experiments the roughness of a Si(100) surface is about 7 nm after sputtering off 50 μm [9], but GaSb has a roughness of about 30 nm after only 500 nm of sputtering [8].

As a step toward addressing sputtering dynamics in systems with more than one species we propose a theoretical description of sputtering in an inhomogeneous system by considering sputter roughening in a solid that consists of randomly distributed impurity atoms embedded in a substrate that sputters off faster than the impurity. We are interested in the evolution of a surface where in addition to the surface shape dependence the sputtering yield also depends upon the atomic or molecular species; i.e., given the same amount of energy imparted to the surface atom the probability of a successful sputtering event varies from one species of particles to another. When an impurity atom is "uncovered" by sputtering it pins the surface until it diffuses away or is finally sputtered away. The rate at which impurity atoms in the bulk are uncovered by sputtering depends upon the local surface curvature and, conversely, the evolution of the surface shape is affected by impurity pinning. Thus, pinning due to an impurity atom leads to a local surface curvature that is more negative than the neighboring parts of the surface. This pro-

*Corresponding author. chmkhc@nus.edu.sg

vides the physical basis for the coupling between the surface impurity concentration and the surface shape.

We propose a model to describe the pinning by coupling the surface height evolution to the surface impurity "concentration" evolution. Results of numerical simulations are presented to show that the shape and growth kinetics of the nanostructures that are formed depend upon both material properties and sputtering flux. This suggests the possibility of tuning the shape and size of nanostructures formed through sputtering. To provide a motivation for the model, we start by considering the Kuramoto-Sivashinsky equation

$$\frac{\partial h}{\partial t} = \nu \nabla^2 h + \frac{\lambda}{2}|\nabla h|^2 - \mu - \kappa \nabla^4 h + \eta. \tag{1}$$

The first and second terms describe the surface-shape dependence of the local sputtering yield, the third term μ is the constant average erosion rate, the fourth term is the surface diffusion contribution, and the final term is the δ-function-correlated noise that models the stochastic nature of the sputtering impact:

$$\langle \eta(x,t) \rangle = 0, \tag{2}$$

$$\langle \eta(x,t)\, \eta(x',t') \rangle = D \delta^d(x-x')\, \delta(t-t'). \tag{3}$$

D is the magnitude of the noise, and d is the dimension of the surface. We study only the $d=1$ case in this paper.

The general approach in converting a microscopic model to a continuum one is clear even if the rigorous mathematical derivation is frequently intractable. The master equation is approximated by the Fokker-Planck equation through a Kramers-Moyal expansion. Then the Langevin equation is obtained. Along the way it generally has to be presumed that the discrete height variable that determines the transition rates in the master equation can be replaced by an appropriate continuous variable. This is usually done through an expansion in powers of the lattice constant. The same procedure would have to be applied to the impurity concentration here, a procedure that typically is not trivial in microscopic models of surface roughening. Here we propose some heuristic but physically motivated modifications to the KS equation to couple the evolution of the surface height to the evolution of the impurity surface concentration. The model we study is described by

$$\frac{\partial h}{\partial t} = f(m)\left[\nu \nabla^2 h + \frac{\lambda}{2}|\nabla h|^2 - \mu \right] - \kappa \nabla^4 h + \eta, \tag{4}$$

$$\frac{\partial m}{\partial t} = g\left(-\frac{\partial h}{\partial t}\right) m \frac{\partial h}{\partial t} + \nu_m \nabla^2 m + \eta_m. \tag{5}$$

The factor $f(m)$ accounts for the effect of an atomically inhomogeneous surface upon the sputtering yield. It models the dependence of the local sputtering yield (described by the first three terms in the KS equation) upon the variable m which describes a generic (coarse-grained) impurity "concentration," possibly an atomic species or defect or an order parameter that affects the sputtering probability. In our work we use $f(m) = \frac{e^{-\gamma m}}{e^{-\gamma m} + e^{\gamma m}}$ where m ranges from $+\infty$ to $-\infty$ with $m=0$ corresponding to the bulk value of the impurity concentration, although other similar functions of m would also be appropriate. The bulk value of m is set to zero for simplicity since the focus is on departures from the bulk concentration. The functional form of $f(m)$ with unbounded values of m is convenient compared to a form that has upper and lower bounds on m for numerical stability. The factor $g(x)$ is the Heaviside function of x. The noise term η_m is also δ-function correlated with the same noise magnitude as η—that is,

$$\langle \eta_m(x,t) \rangle = 0, \tag{6}$$

$$\langle \eta_m(x,t)\, \eta_m(x',t') \rangle = D \delta^d(x-x')\, \delta(t-t'). \tag{7}$$

We choose this as the correlation in m in order to model a bulk that has a randomly distributed impurity, η_m simulating the effect of impurities "surfacing" at random positions on the surface as the particles above them are sputtered away. The time-averaged value of η_m for each position is set to zero since this is the average impurity concentration in the bulk. There is clearly a difference between this model for sputtering impurity noise and systems such as GaSb and InP. In these latter systems, the two species are found in ordered arrays. This ordering might be better represented by a spatially ordered noise term.

The parameter γ controls the degree of inhomogeneity of the surface with respect to the probability of sputtering. When γ is zero, the sputtering yield is independent of m, the sputtering probability is independent of the species, and the height evolution equation reduces to the Kuramoto-Sivashinsky equation. When γ is large, the sputtering probability varies rapidly when m changes sign. Where the surface impurity concentration is larger than the bulk (positive m), we expect the sputtering probability to go rapidly to zero as m increases, thus pinning parts of the surface. The evolution of these parts of the surface is governed by only the Mullins diffusion and noise terms. Indeed, when the parameter γ is infinitely large, Eqs. (4) and (5) decouple and the height evolution is controlled by the linear molecular beam epitaxy (MBE) equation. We discuss this limit again below.

The first term in the evolution equation for m is motivated as follows: at points on the surface where the local velocity is negative, the variable m is driven towards zero (the bulk value for m) at a rate that depends upon the local sputtering velocity. The higher the local sputtering velocity, the more rapidly m is driven towards the bulk value of zero. The second term accounts for "concentration" driven surface diffusion of m. There can be additional nonlinear corrections to the diffusion of m. For instance, since the amount of energy delivered per unit local surface area depends upon the slope, the diffusivity of m is expected to depend upon the gradient of h. This will introduce an additional coupling between m and h that is not due to the sputtering probabilites of the two different species. The diffusion coefficient of m can also depend upon the local impurity concentration itself; this would be relevant when the lateral interaction between the impurity atoms is important. We discuss these additional terms below. The third term in the evolution equation for m models the random distribution of the impurity in the bulk. The model is simulated using fourth-order Runge-Kutta integration.

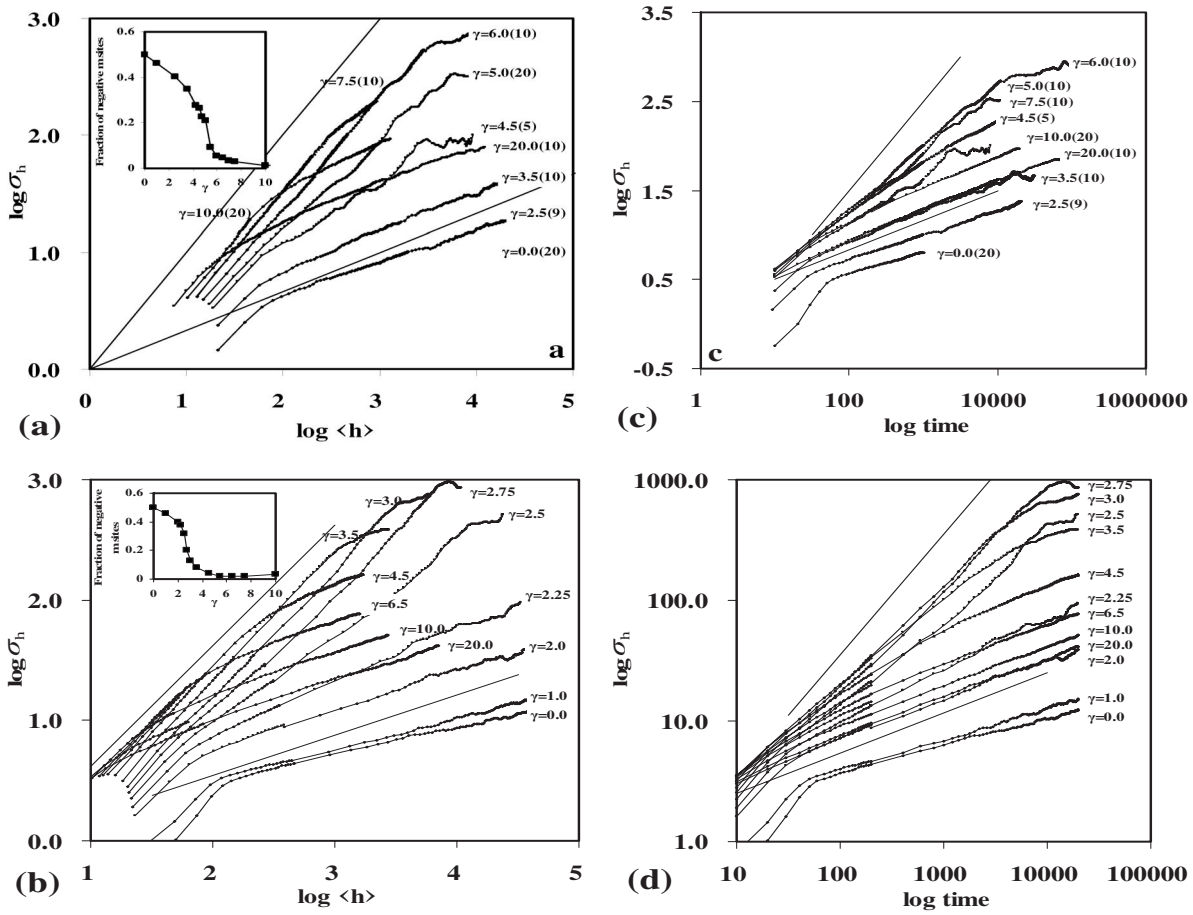

FIG. 1. (a) and (b) Roughness σ_h is plotted versus the average number of layers sputtered off for different γ values with ν, λ, κ, and D all equal to 1, μ equal to 5, and the bulk impurity concentration equal to 0.005. The diffusivity of the impurity is controlled by ν_m which is set equal to one in (a) and 0.1 in (b). These results are obtained from simulations with system size of 5000; the number of simulation runs for each γ is indicated in the brackets. The inset shows the average fraction of the surface with negative m—that is, parts of the surface where the impurity concentration is lower than the bulk impurity concentration. In (c) and (d), the abscissa is time instead of the average number of layers sputtered. The linear rapid-roughening regime is observed and the asymptotic growth exponents are the same as in (a) and (d). The trendlines have slopes equal to 1 and 1/3.

Results showing the dependence of roughness $\sigma_h=(\langle h^2\rangle - \langle h\rangle^2)^{1/2}$ upon the number of sputtered layers are plotted for two different impurity diffusivities $\nu_m=1.0$ and $\nu_m=0.1$ in Figs. 1(a) and 1(b), respectively. Our simulations are carried out with periodic boundary conditions on lattices of size 5000 units. The number of simulation runs for each γ is indicated in brackets in the figures. At early times, roughness increases almost linearly with time. For small γ, meaning that the local sputtering probability is not strongly dependent upon the impurity concentration, the initial roughening regime quickly crosses over to a slower roughening regime. With γ equal to zero, the roughening exponent β decreases to approximately 0.22 and 0.23 for $\nu_m=1.0$ and $\nu_m=0.1$, respectively. These estimates are best-fit exponents obtained using the average roughness of 20 simulation runs each. This slow-roughening regime is reached even at a low roughness of only approximately 3 units. However, as γ increases, the growth exponent for this slow-roughening regime increases until $\beta\approx 1$. For the higher surface diffusivity of m where $\nu_m=1$ [Fig. 1(a)], a growth exponent of $\beta\approx 1$ is reached when γ is approximately equal to 5, whereas for the lower-diffusivity case where $\nu_m=0.1$ [Fig. 1(b)] this is reached when γ is approximately equal to 2.75, indicating that for lower impurity diffusivity, the onset of rapid roughening requires a smaller local sputtering inhomogeneity.

For $\gamma=5.5$, rapid roughening is observed for roughness (number of sputtered layers) up to 10^3 (10^4) with impurity diffusivity ν_m equal to 1. With ν_m equal to 0.1, rapid roughening is also observed over a similarly large range of roughness and number of sputtered layers for γ approximately 2.5–3.5. It is clear that for large and for small γ values, the rapid-roughening regime crosses over to a regime with a smaller value of β at sufficiently long times. However, the long-time behavior for intermediate γ values is not as clearly established in the simulations. For γ values between approximately 5 (2.5) and 6 (3.5) with $\nu_m=1.0$ (0.1) the rapid-roughening regime is apparent until close to the ends of the simulations. For these intermediate γ values the regime where the roughening crosses over to smaller β is too short to definitively quantify the growth exponents. Longer simulations on larger lattices are probably needed to address this

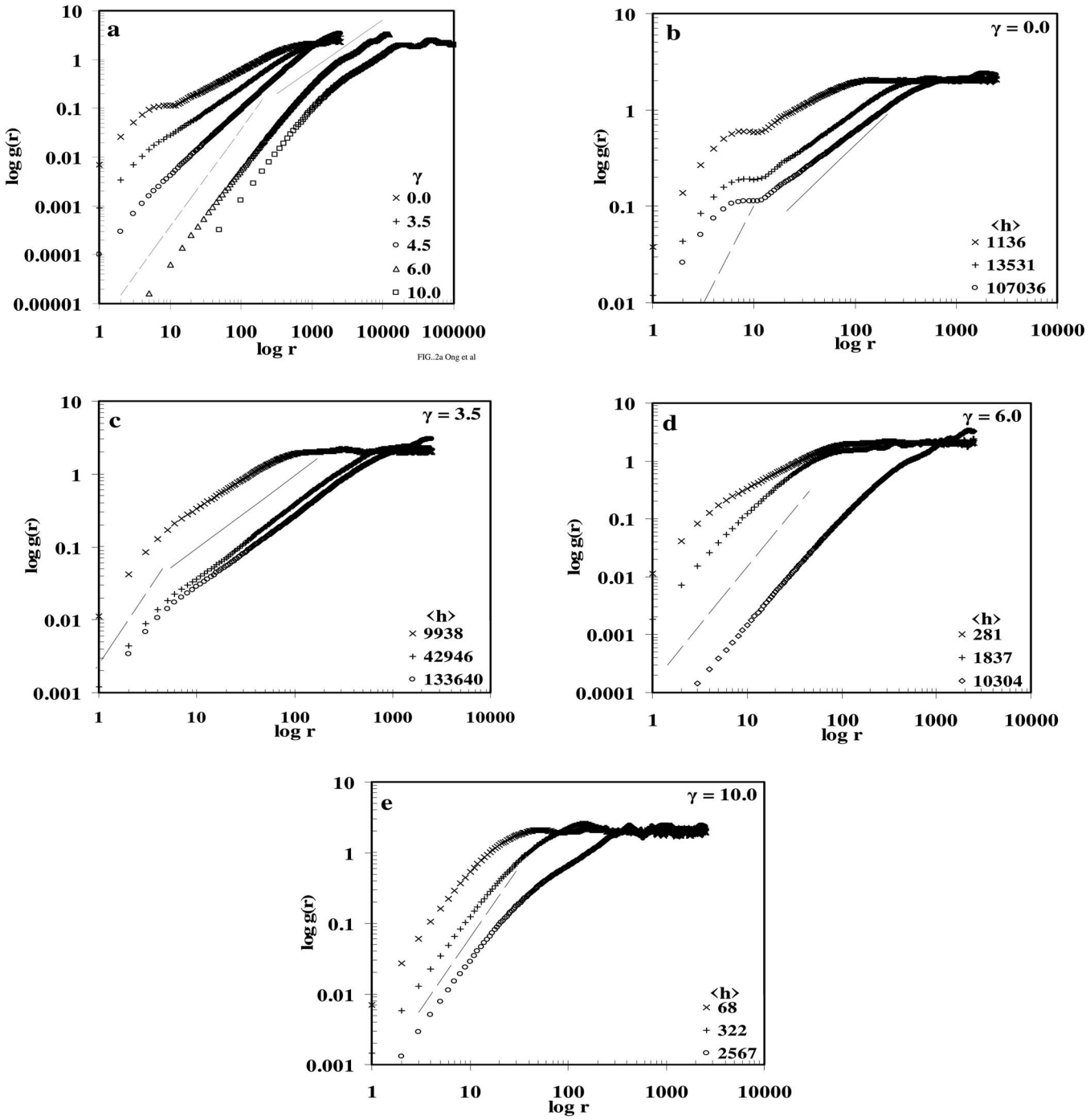

FIG. 2. The height-height correlation versus lateral length is plotted in (a) for a number of different γ values. In (b), (c), (d), and (e) the time dependence of this height-height correlation for specific γ values is shown. The two trend lines correspond to roughening exponents of 1 and 1/2. Note that the slope of the correlation as plotted is twice the roughening exponent α.

issue. The long-time slow-roughening regime is accessible in our $\nu_m=1.0$ (0.1) simulations for γ larger than approximately 6 (3.5) and appears to have a Kardar-Parisis-Zhang (KPZ) exponent. For $\nu_m=1.0$, the growth exponent is approximately 0.34 for $\gamma=20.0$ [see Fig. 1(a)], while for $\nu_m=0.1$ the observed growth exponents are 0.40, 0.35, and 0.34 for γ equal to 4.5, 5.5 (not plotted), and 6.5, respectively, at the ends of the respective calculations [Fig. 1(b)]. Our results show that there is an intermediate-time growth regime where the growth exponent changes from approximately 1/4 to unity as γ increases from zero. For γ values in a range that depends upon the value of the impurity diffusivity ν_m, this rapid roughening can persist for roughness up to 10^3. At long times there is a crossover to the KPZ growth exponent, observable in our simulations at least for large γ.

We have examined the dependence of surface roughness upon the average number of sputtered layers. It is, however, not clear that the average number of sputtered layers is lin-

early proportional to time in the two-field model studied here. Thus, we plot the roughness as a function of time instead of the number of sputtered layers in Figs. 1(c) and 1(d). The data in Fig. 1(c) [1(d)] correspond to those plotted in Fig. 1(a) [1(b)]. The same asymptotic growth exponents are obtained. In addition, a linear dependence of the roughness upon time is also observed for the rapid-roughening regime discussed above.

The height-height correlation on the surface is studied using the quantity $g(r)=\sigma_h^{-2}\langle[h(r_0)-h(r+r_0)]^2\rangle$, where the average is computed over all positions r_0. In Fig. 2(a) we plot the correlation function $g(r)$ at the end of the simulations for some values of γ. In Figs. 2(b), 2(c), 2(d), and 2(e) we plot this correlation at different times for γ equal to zero, 3.5, 6.0, and 10.0, respectively. For short times and short lateral length scales, the roughening exponent estimated using this data is close to unity for all values of γ. Note that, considering the definition of $g(r)$ above, the roughening exponent is equal to one-half the slopes obtained in these plots. This scaling at short length crosses over to a roughening exponent of about 0.44 for γ equal to zero for length scales larger than approximately 10. This roughening exponent gradually increases with γ. For γ equal to 3.5, 4.5, and 6.0, α is approximately 0.5, 0.74, and 0.98, respectively. For γ equal to 4.5 (not shown in Fig. 2) this roughening exponent persists up to length scales of 10^3. However, with even larger values of γ, a long-time and long-length scaling regime is observed. In Figs. 2(d) and 2(e) for γ equal to 6.0 and 10.0, this is seen for the height-height correlation obtained at the longest time accessed in our simulations. The long-length scale regime is observed when lateral lengths of longer than approximately 10^3 are considered. The roughening exponent α is approximately 0.48 in this regime, which is in good agreement with the KPZ exponent.

We note that the long-time growth exponent accessible in the large-γ calculations is not the value expected for Mullins diffusion although much of the surface is expected to be higher in impurity concentration and have a time dependence dominated by the Mullins diffusion and the noise terms. In the inset of Figs. 1(a) and 1(b), we plot the average number of surface sites with negative values of m as a function of γ. Even for the largest values of γ in our calculations, there are still surface sites with negative m, and thus, have sputtering probabilities close to unity for large γ although these amount to only 3% of the surface. Thus, the Mullins term does not dominate the sputtering terms over the entire surface in Eq. (4) even for the largest values of γ used here. The simulation results show that both α and β are close to KPZ values. As noted above the surface evolution is governed by the linear MBE equation when γ is infinite and in which case Eqs. (4) and (5) are decoupled. However, the simulation results with our largest values of γ are not consistent with linear MBE kinetics, suggesting that the $\gamma=\infty$ limit may be singular.

In Figs. 3(a) and 3(b) we plot the dependence of the fluctuation in the surface impurity concentration $\sigma_m=(\langle m^2\rangle-\langle m\rangle^2)^{1/2}$ upon γ; Fig. 3(a) is for $\nu_m=1.0$ while Fig. 3(b) is for $\nu_m=0.1$. The averages are taken over the surface at the last iteration of the simulation results in Figs. 1(a) and 1(b). Comparing the results (for $\nu_m=1.0$) in Fig. 3(a) to the roughness plots in Fig. 1(a), we see a correlation between the sharp increase in σ_m and the onset of rapid roughening. Both the growth exponent β and the impurity fluctuation σ_m increase sharply for γ approximately equal to 5 and then decrease gradually when γ is increased to larger values. For γ equal to 10 or 20, σ_m is considerably smaller. A similar correspondence holds for the $\nu_m=0.1$ data shown in Fig. 3(b) and the roughness plots in Fig. 1(b).

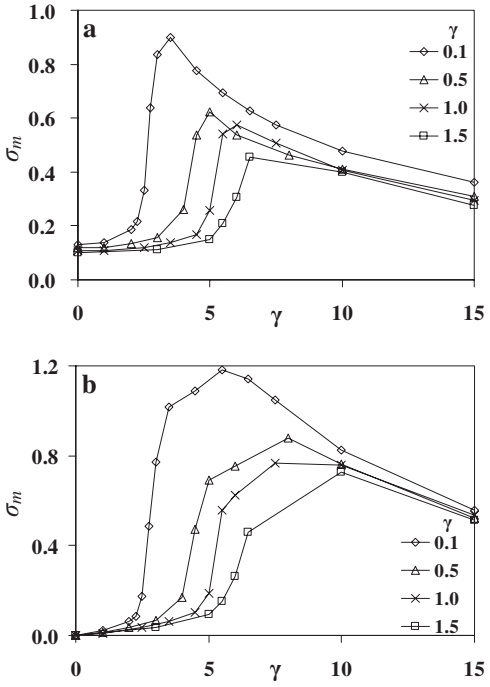

FIG. 3. Here we plot the dependence upon γ of the fluctuation σ_m in surface impurity concentration. (a) is for $\nu_m=1.0$ while (b) is for $\nu_m=0.1$, corresponding to the roughness time-evolution shown in Figs. 1(a) and 1(b), respectively. These graphs show the correlation between the onset of rapid-roughening, seen in Fig. 1, and large surface fluctuation in impurity concentration when γ is increased from zero.

We plot in Figs. 4(a)–4(d) the surface profiles for $\gamma=6.0$ and zero. Figures 4(a)–4(c) are surface profiles corresponding to the $\gamma=6$ results plotted in Fig. 1(a), while Fig. 4(d) is for the $\gamma=0$ data in Fig. 1(a). Note the relative scales of the horizontal and vertical axes. In Fig. 4(d) for γ equal to zero, we include an inset where the scales for the horizontal and vertical axes are the same in order to illustrate the curvature of the structures at the surface. The surface structures for $\gamma=6$ are distinctly conical and have large roughness, while those observed for $\gamma=0$ are more rounded and have much lower roughness. To illustrate the relationship between the surface structure and the variation of the *local* surface impurity concentration, we plot in Fig. 4(a) the surface profile and the concentration parameter m at early times (number of sputtered layers is 100) for $\gamma=6.0$. This is in the top left panel. Parts of the surface where m is large, implying a high concentration of the impurity, have curvatures that are more negative than average. This correlation decreases with time as illustrated in the bottom left panel of Fig. 4 for 1000 sputtered layers.

The correlation between the dependence of the fluctuta-

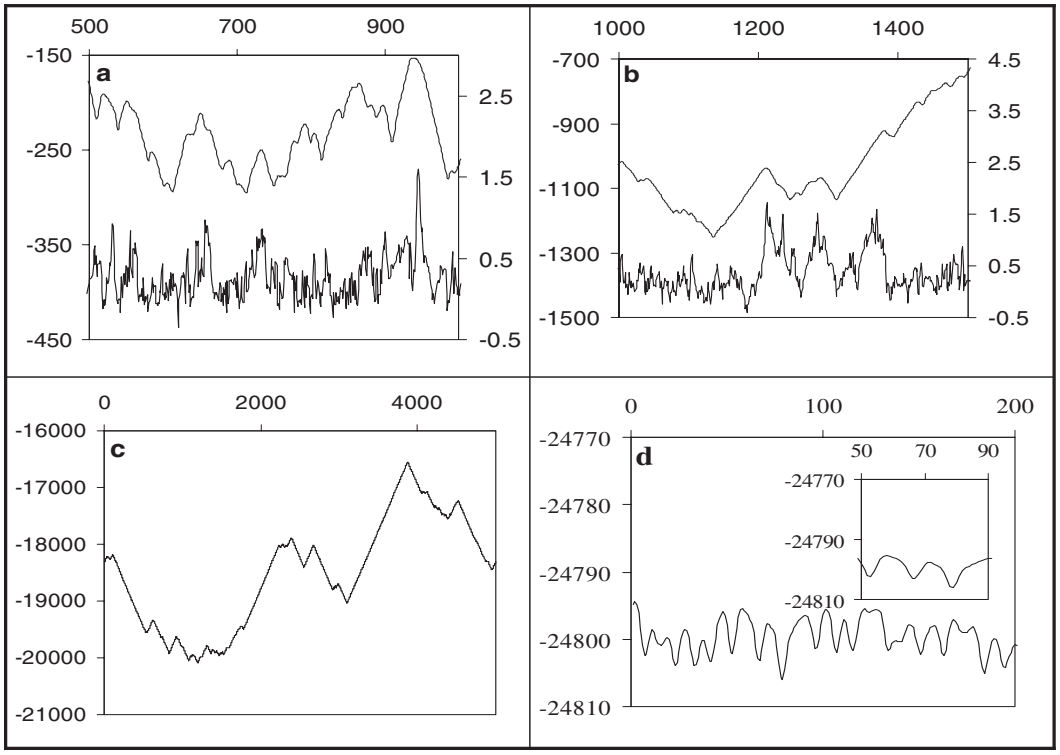

FIG. 4. The surface height for different γ values is plotted here. (a), (b), and (c) are for $\gamma=6$; (d) is for $\gamma=0$. The left vertical axis is the height (with the surface height initially equal to zero), showing the average number of layers sputtered off. For (a) and (b) the value of m (right vertical axis) is also plotted to illustrate the relationship between the surface curvature and the local impurity concentration. The ratio of roughness to the number of layers sputtered is much larger for $\gamma=6$ than for $\gamma=0$. The inset of (d) shows part of the surface using the same scale for the horizontal and the vertical axes to illustrate the shape of the surface structures.

tions in m upon γ shown in Fig. 3(a) and the change in the roughening kinetics with γ shown in Figs. 1(a) and 1(b) can be understood as follows. If a small fluctuation in the impurity occurs at a point on the surface, the local curvature there becomes negative because of the lower probability of a successful sputtering event. The negative curvature then reduces the local sputtering rate further because of the surface curvature dependence of the sputtering dynamics. Conversely, a point with a low local concentration of the impurity is likely to develop a positive curvature which then further increases in curvature as a result of the curvature dependence of the sputtering dynamics. Therefore, we think of the roughening surface as consisting of segments of two different types, one of which erodes rapidly and has a large positive curvature, and the other of which erodes slowly because of impurity pinning due to a positive fluctuation in the local concentration of the impurity. This same impurity-pinning role has been suggested for agglomerates of indium, which sputter off less rapidly than phosphorus from InP, thereby acting as seeding points for the observed conical nanostructures [7]. The crucial point is that correlation rapidly develops between fluctuations in the local concentrations of the impurity and the local surface curvature.

Our simulations are for $d=1+1$, but our argument for the kinetics in the rapid-roughening regime is independent of dimension. Thus, in $d=2+1$, we also expect a growth exponent in the rapid roughening regime that is close to 1. To investigate this we carried out calculations for the $d=2+1$ case. System sizes of 400×400 are used in the calculations. In Fig. 5(a) roughness is plotted against the number of sputtered layers for $\gamma=0$, 5, 7.5, 10, and 15, all with the coefficient of the nonlinear term λ set equal to 1. As in the $d=1+1$ simulations, there is an initial rapid-roughening phase when the surface is atomically smooth. We observe a crossover to a slow-roughening regime for all γ values. Considering first the case of γ equal to zero, the results in Fig. 5(a) show that the initial rapid roughening is not power law but can appear to have a time dependence that is exponential. If we estimate the (effective) growth exponent in the slow-roughening regime, we obtain a value of less than 0.1 for $\gamma=0$. Since the time-evolution equation reduces to the KS equation for γ equal to zero, this result suggest that the long-time growth exponent for the KS equation in $d=2+1$ is significantly below the KPZ value. This kinetic behavior is consistent with what is known about the KS equation—that is, rapid initial roughening followed by a long intermediate regime with Edwards-Wilkinson scaling before KPZ scaling is observed exponentially [2,4]. It is also consistent with our previous rather different Monte Carlo simulations of an atomistic model which found that sputter roughening scales logarithmically at sufficiently large times [19] and also with recent experimental data [20]. There is, so far, no direct numerical verification of the asymptotic KPZ scaling for $d=2+1$, although there is analytical [21] and direct numerical evidence [4,22] for $d=1+1$. Our calculations here are not able to access large values of roughness and, therefore, the

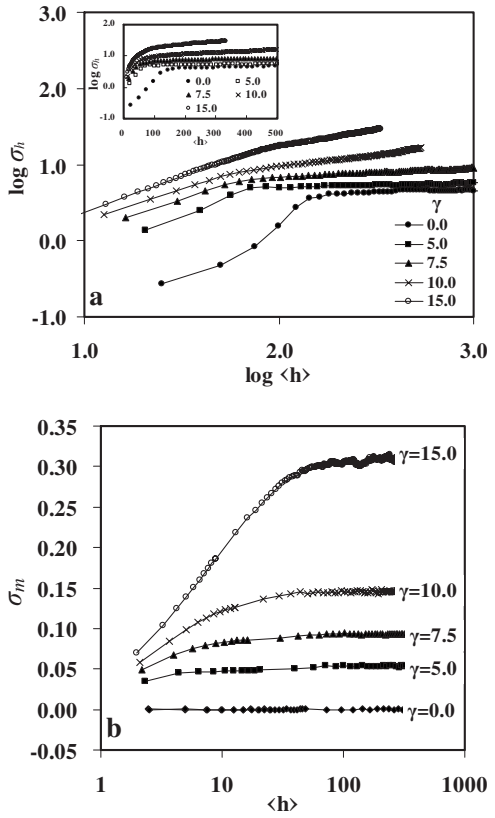

FIG. 5. The dependence of the roughness upon the number of sputtered layers is plotted here for $d=2+1$ simulations. The parameters used in the simulations are λ, ν, κ, and ν_m all equal to 1. The graphs are labeled with the corresponding γ values. The inset of (a) shows the same data plotted using logarithmic-linear axes. In (b) the corresponding time dependence of the fluctuation in m is plotted for each γ.

results do not even probe the intermediate logarithmic scaling for $d=2+1$ conclusively.

It is clearly seen in Fig. 5(a) that as γ increases the observed growth exponent increases, as was observed above for $d=1+1$. When γ is increased to 15, the initial roughening regime has a growth exponent of approximately 0.95; this crosses over to a regime with a growth exponent of approximately 0.39. We check for finite-size effects using calculations with a system size of 800×800 for $\gamma=10$. The data for both 800×800 and 400×400 agree very well up the roughness simulated. In order to examine this crossover in roughening kinetics, we plot the evolution of the fluctuation σ_m against the number of sputtered layers in Fig. 5(b). As in the $d=1+1$ case, the long-time value of σ_m increases as γ increases; for the range of γ we investigated this increase in the fluctuation of m is correlated with the increase in the growth exponent. We also note that the initial rapid increase in the fluctuation of m is correlated with the initial rapid roughening. The crossover to a smaller growth exponent occurs when the growth of σ_m slows down. Thus, as in $d=1+1$, we observe an interesting correlation between the impurity concentration fluctuation and the roughening kinetics. There is a clear dependence of the observed growth exponents upon the surface inhomogeneity.

To provide further characterization of the surface profiles in the model, we plot in Fig. 6 the surface profiles for the $d=2+1$ simulations for different γ, corresponding to the results in Fig. 5(a). The corresponding height-height correlations quantified through $g(r)$ are plotted in Fig. 7. No distinct power-law behavior is observed. The roughness observed in all our $d=2+1$ simulations is not large as compared to the $d=1+1$ simulations. However, we have not explored the parameter space for the $d=2+1$ model as much as we have done for the $d=1+1$ model. It is important to note that the surface profiles obtained in both the $d=1+1$ and $d=2+1$ simulations of the model are noisier than the surfaces observed in sputtering experiments. In Fig. 8 we plot the height of the surfaces obtained in our simulations in gray scale. By comparing these top view plots of the surface in the $d=2+1$ simulations and the plots in Figs. 4 and 6 against the surface profiles observed experimentally (Fig. 1 in each of Refs. [7,8]) it is seen that the model investigated here produces a considerably more disordered surface although cellular structures are observed. There is greater noise in the height variations and is also in the in-plane variation. In particular, clearly hexagonally ordered features are observed in Refs. [7,8]. This is also the case in Monte Carlo simulations of a particle model for sputtering where a hexagonal symmetry is also observed for the in-plane ordering (see Figs. 3 and 4 in Ref. [19]). In contrast, a previous numerical simulation of the KS equation with somewhat extended simulation runs resulted in surface profiles that are considerably noisier [23]; no clear hexagonal ordering was observed (see Figs. 2 and 13 in Ref. [23]). This lack of in-plane ordering was also observed in the numerical simulations by a different group [24]. The noisy nonlinear pattern formation in these simulations in contrast to the long-range order observed in sputtered InP and GaSb surfaces shows that the latter are probably fundamentally different from the nonlinear models investigated.

Two growth regimes have been clearly observed in experimental data for InP sputtering [7]. Initially indium-island agglomeration and mound coarsening occur with a growth exponent of approximately 0.8 [7], which is probably dominated by different surface velocities of the indium-enriched islands compared to the InP substrate. The observed growth exponent decreases in the late stage of sputtering to a value of approximately 0.27. Interestingly, our calculations for $\gamma=10$ [Fig. 5(a)] show almost exactly the same growth exponents even though the morphologies are clearly different. It has been suggested that the initial rapid growth corresponds to indium accumulation and agglomeration at the surface. When this process slows down slower roughening is observed. That is, the late-time growth exponent of 0.27 is attributed to the evolution of a surface with a fairly uniform indium concentration. However, in our model the crossover corresponds to a close to saturation of the surface inhomogeneity. Therefore, within our model the late-time roughening kinetics is due to the time evolution of a surface that is inhomogeneous but for which the inhomogeneity is not rapidly changing with time as in the early time rapid-roughening regime.

In contrast to the two power-law regimes observed for $\gamma=10$, the simulations for small γ show an initial exponential

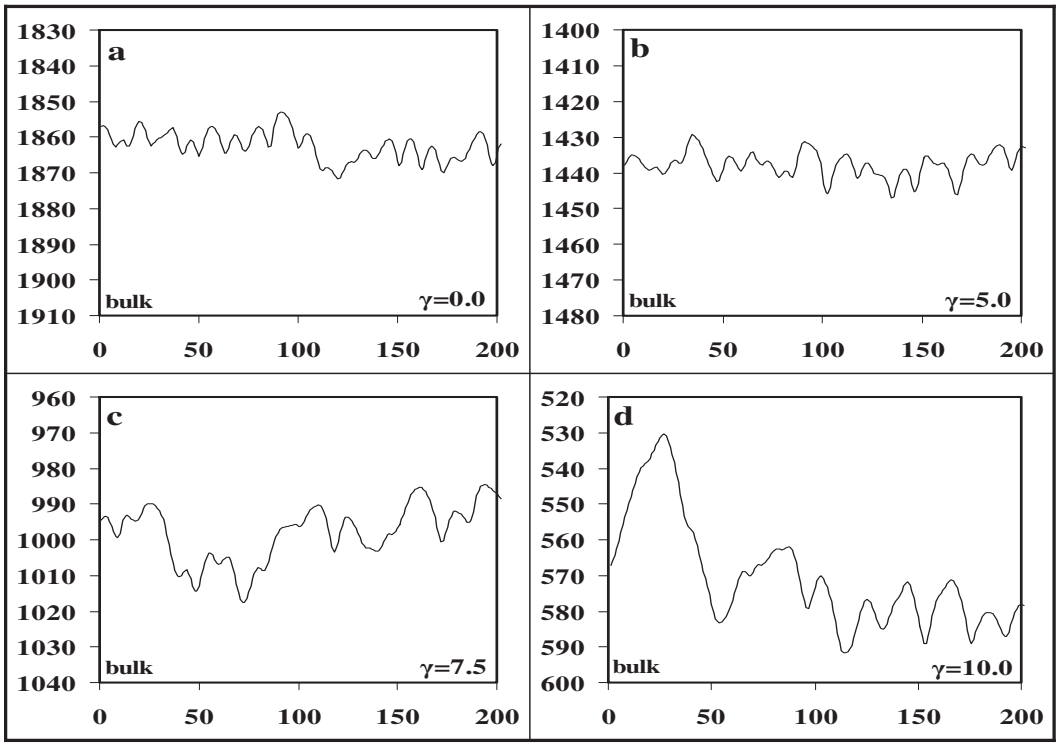

FIG. 6. Surface profiles from $d=2+1$ simulations. These are profiles obtained at the end of the corresponding simulations for the roughness data plotted in Fig. 5(a). The entire surface for each of these profiles is shown in the corresponding panel in Fig. 8.

roughening that rapidly saturates. In particular, for γ equal to zero, we observe a short initial rapidly roughening regime that is followed by a regime with a small growth exponent of 0.1 as discussed above. In order to better characterize the initial rapidly roughening regime, we performed a set of $d=1+1$ calculations where we reduced the coefficient of the nonlinear term from λ to 0.1. This means that the initial linear instability is stronger and local fluctuations in surface height are more likely to grow in amplitude. Plots of the roughening kinetics are shown in Fig. 9(a); the same data are plotted with logarithmic-linear axes in the inset of Fig. 9(a). When the stabilizing nonlinear term is small, the initial roughening is determined by the instability due to the negative effective surface tension in the KS equation leading to rapid roughening as expected [2,4]. The results obtained here for $\lambda=0.1$ are consistent with this. The crossover to very slow growth after this initially rapid-roughening regime is also consistent with the KS equation having a long preasymptotic regime where Edwards-Wilkinson behavior ($\beta=0$ for $d=2+1$) is observed [2,4].

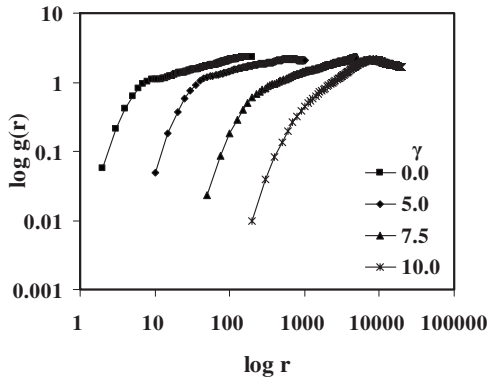

FIG. 7. Height-height correlations in $d=2+1$ corresponding to the roughness data plotted in Fig. 5(a).

In Fig. 9(b), we plot results of similar calculations in $d=2+1$ for γ equal to zero and for various magnitudes of the nonlinear term. Since γ is equal to zero, the model reduces to the KS equation here and the results we obtain here are in agreement with what is known about the KS equation. For the λ values investigated, the long-time growth exponent in $d=2+1$ for small γ is rather small as is the case for the $\lambda=1$ simulation plotted in Fig. 5(a). The results shown in Fig. 9(b) suggest that the long-time growth exponent is not strongly dependent upon the size of the nonlinear term but the asymptotic value of the roughness grows as λ decreases. Thus, the initial rapidly roughening regime persists longer for smaller λ values. It is clear from the results in Figs. 9(a) and 9(b) that the initial kinetics for small γ values is not described by a power law. The same data are plotted using logarithmic-linear axes in the inset, showing that the initial time dependence of roughening is also not exponential over the entire regime. It is known for the KS equation that the kinetics is exponential over a part of the initial roughening regime when the nonlinear term is small. Our results are in agreement with this since for γ equal to zero, the model reduces to the KS equation.

The results in Fig. 9(a) show that the initial apparently exponential behavior changes to a power-law behavior when the surface inhomogeneity (and γ) is sufficiently large, thus suggesting that in mixed systems, there is a competition between linear-instability-driven roughening and impurity-

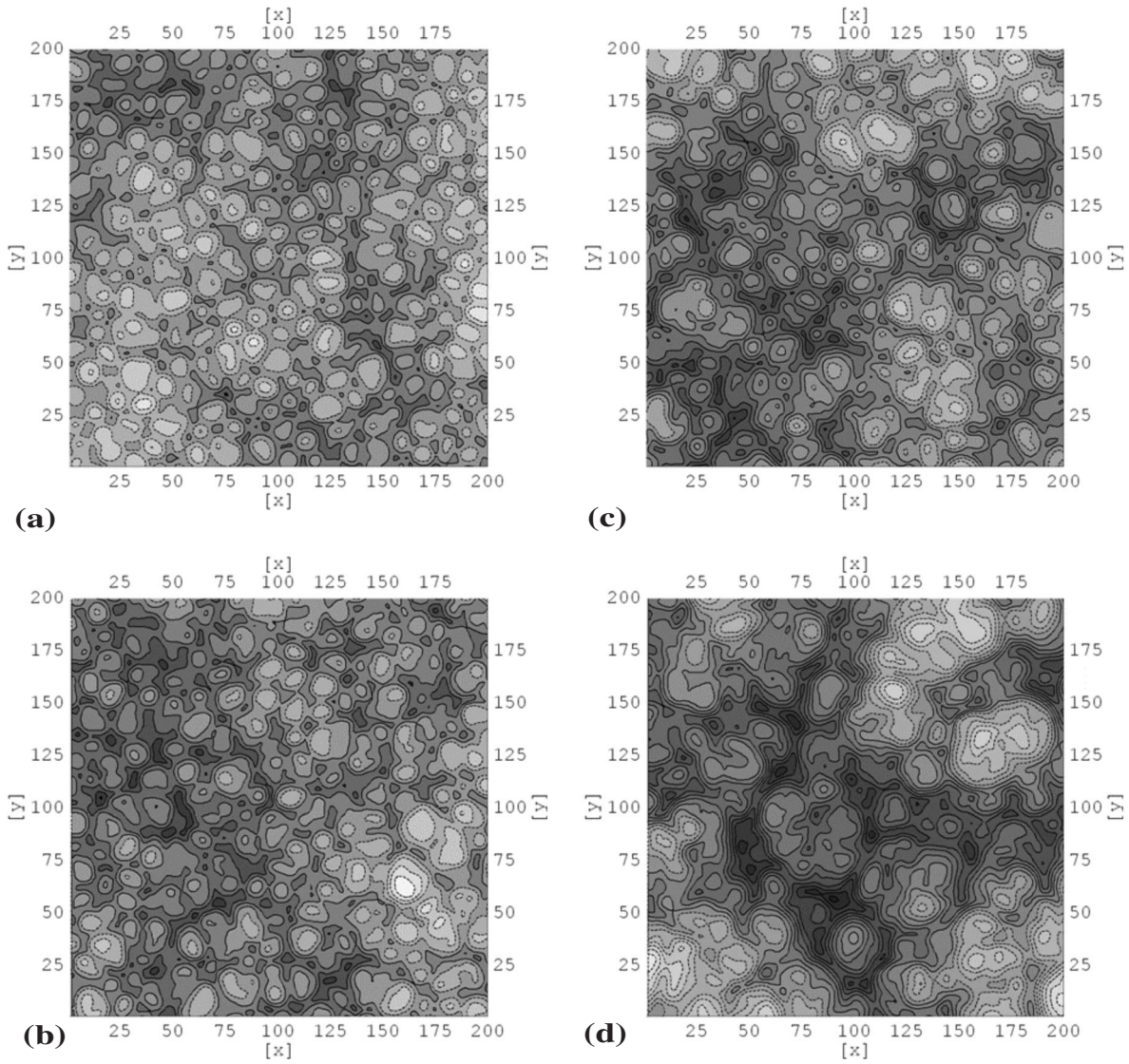

FIG. 8. Gray scale plots of the surfaces obtained in our $d=2+1$ simulations. The solid contours are heights below the average height while the dotted contours are heights above the average height in each figure. The height interval between contours is 5 units for (a), (b), and (c) and 10 units in (d). A cross section of each of these surfaces is shown in the corresponding panel in Fig. 6.

pinning roughening during the initial roughening stages. Thus, our calculations show that the observed roughening kinetics depends upon the surface inhomogeneity. The experimental roughening kinetics shows that in GaSb an initial apparently exponential roughening occurs and the roughness rapidly saturates. One the other hand, in InP roughening is described by power laws both initially and for longer times with exponents approximately 0.8 and 0.27, respectively. Therefore, within our model, GaSb corresponds to low γ (less the inhomogeneous surface) while InP corresponds to high γ. However, as noted above, the surface morphology observed in the model discussed here is rather different from that observed experimentally, suggesting that the experimental systems are not described by the nonlinear model here even though similar kinetic behaviors are observed.

We can further characterize the inhomogeneity of these surfaces by considering the dependence of the slope distribution upon γ. We consider only $d=1+1$ here. In Fig. 10 we plot the distribution $f(s)$ of the slope s at long times for a range of γ values for the data shown in Fig. 1(a). When γ is low (small inhomogeneity in the sputter probability), the slope distribution has a peak at zero slope. However, when γ is sufficiently large, a peak develops at a nonzero slope, as suggested by the surface profiles in Fig. 4. Note that the peak at a finite slope is much smaller at $\gamma=10$ and $\gamma=20$, as might be expected from the roughening behavior for these γ values. It is interesting to note that at $\gamma=4.25$ a small shoulder at nonzero slope develops in the long-time slope distribution, and by $\gamma=4.75$, the peak at nonzero slope dominates the peak at zero slope. This change in the shape of the slope distribution corresponds to the rapid change in the value of the impurity concentration fluctuation and the rapid-roughening kinetics discussed above. Thus, the onset of the rapid roughening regime is controlled by γ—i.e., by how rapidly the sputtering probability changes with the surface concentration m. However, even though fluctuations in m

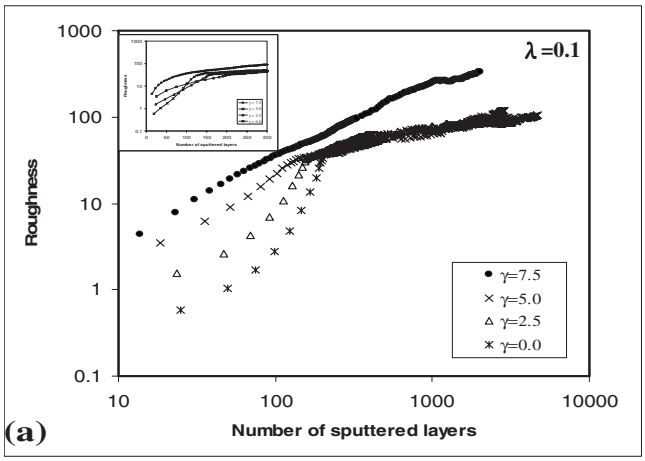

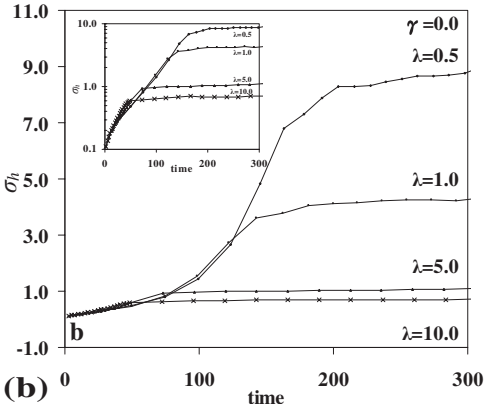

FIG. 9. These figures show the effect of the nonlinear term upon roughening kinetics. In (a) the time dependence of roughness is plotted for $d=1+1$ for λ equal to 0.1; that is, the nonlinear term is smaller than for the results shown in Fig. 1(a). The inset shows the same data plotted on log-linear axes. In (b) results for roughness versus time in $d=2+1$ are plotted for simulations with γ equal to zero and different λ values. In the inset the same data are plotted with logarithmic-linear axes. The results illustrate that the effective exponential-time kinetics for the KS equation ($\gamma=0$) is clearly observed if the nonlinear term is sufficiently small. This crosses over to a power-law dependence for nonzero γ.

control the onset of this regime, the slope of the cones is not strongly dependent upon γ.

In Figs. 11(a) and 11(b), we plot the slope distributions obtained for the different λ and μ values keeping γ constant at a value of 7.5. These results show that the slope of the cones is determined by the coefficient λ of the nonlinear term and the average erosion rate μ. When $\lambda(\mu)$ increases, the slope of the conical structures decreases (increases). In the bottom panels (c) and (d) of Fig. 11, we plot the slope distribution as a function of the rescaled slope $s(\lambda/2\mu)^{1/2}$. These plots show that the peaks for different λ and μ values all occur at a rescaled slope of approximately 1, thus indicating that the slope selected by the sputtering process is equal to $(2\mu/\lambda)^{1/2}$ and depends only upon the nonlinear term and the constant average erosion rate. Thus along the straight sides of the conical structures, the contribution of the nonlinear term exactly balances that of the constant erosion rate.

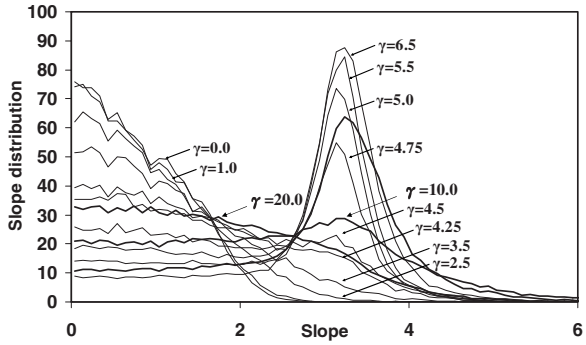

FIG. 10. Plots of the surface slope distribution $f(s)$ for different γ values for the data shown in Fig. 1(a). These slope distributions are obtained when the average number of sputtered layers is 2000. The slope distribution $f(s)$ is normalized to 1.

For cones with slopes smaller than $(2\mu/\lambda)^{1/2}$, the nonlinear term dominates the constant erosion term and the slope increases, and vice versa for steeper cones. Simulations for $\nu=0.01$ produced slope distributions that are rather similar to those for $\nu=1.0$. Thus, at least in this range of ν the selected slope does not depend upon the effective surface tension. We are therefore led to the interesting conclusion that the shape of the conical structures can be selected by tuning the values of μ and λ; both are linearly proportional to the incident sputtering flux but depend differently upon how the sputtering ion energy is distributed about the point of impact [2,6]. In Figs. 12(a) and 12(b), we plot the slope distributions for each γ value in the simulations where the nonlinear term is reduced by setting $\lambda=0.1$. The roughening kinetics is shown in Fig. 9(a). The distributions in Fig. 12(a) are at earlier times, the actual number of layers sputtered for each case being about 400. The distributions plotted in Fig. 12(b) correspond to the largest value of roughness in each of the cases shown in Fig. 9(a). For $\gamma=7.5$ the scaling exponent of close to unity shows that impurity pinning dominates for this value of γ. A sharply peaked maximum in the slope distribution is observed in Fig. 12(b) at a slope of 10, as we have seen from earlier arguments. For the other values of γ, the slope distribution does not change significantly between 400 sputtered layers and up to 5000 sputtered layers. In contrast to the $\gamma=7.5$ case, no peak is seen at slope $s=10$ although the distributions show a shoulder between $s=10$ and $s=15$.

For simplicity, we have not included other possible terms in our model. There are other effects that can play a role in sputtering aside from the usual terms in the KS equation and the impurity-concentration-dependent sputtering probability that we have introduced here. For instance, with a sputtering flux normal to the surface, the concentration of particles hitting the surface is dependent upon the local slope of the surface. This induces a thermally activated height diffusion current proportional to the $\nabla^2(\nabla h)^2$ [17] that is due to the concentration gradient of the sputtering particles. This rescales as $b^{\alpha+z-4}$ where b is the length scale, and α and z are the roughness and dynamic exponents, respectively. This is expected to be less relevant than $|\nabla h|^2$ or $\nabla^2 h$. However, this nonlinear term has been included in recent work on pattern formation in amorphous metal alloy films [17,18]. The equation used (Eq. (2) in Ref. [18]) is the KS equation with this

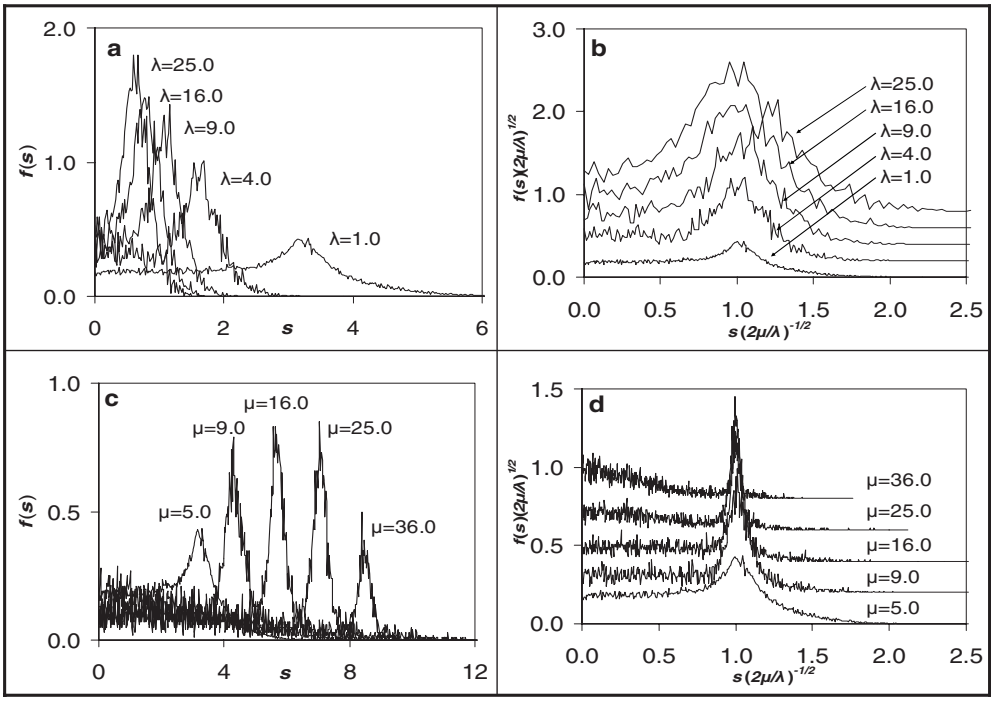

FIG. 11. Plots of the surface slope distribution for $\gamma=7.5$. (a) and (b) show results for different λ values for the same set of parameters as in Fig. 1(a). Similarly, (c) and (d) show results for different μ values. In (b) and (d) the horizontal axis is $s(2\mu/\lambda)^{-1/2}$ and the vertical axis is $f(s)(2\mu/\lambda)^{1/2}$; the graphs are displaced vertically in steps of 0.2 for clarity.

additional nonlinear term. By optimizing the coefficients of the four terms in the time-evolution equation, the experimental results can be fitted well, suggesting that this nonlinear correction to surface diffusion can be important. Earlier work on the effect of the term proportional to $\nabla^2(\nabla h)^2$ shows that it stabilizes the growth of the unstable modes arising from the linear terms in the KS equation [17]. We expect such a term to have a similar qualitative effect as the usual nonlinear term in the KS equation as in Figs. 9(a) and 9(b); that is, a smaller nonlinearity results in a longer time and a greater surface roughness before the crossover to the slow-roughening regime. Another effect that we have not considered here is the dependence of the diffusion of m upon the local surface shape. Just as the slope dependence of the concentration of sputtering particles induces a height-diffusion current, it also results in a slope dependence for the diffusivity of m, resulting in the terms $|\nabla h|^2\nabla^2 m$ and $m\nabla^2(\nabla h)^2$. For slopes $s \gg 1$, the geometrical dependence of the surface distance upon slope also requires a correction term of the form $|\nabla h|^2\nabla^2 m$. We also expect other terms that are nonlinear in m to occur. For instance, if we consider interactions between impurity particles, the time evolution of m can be described by the Ginzburg-Landau equation along with the first term in Eq. (5) to account for the effect of sputtering upon m.

In summary, we have presented a theoretical description of sputtering dynamics for surfaces where the local sputtering yield depends through a surface "concentration" upon variations in the sputtering probability of the species present. The model consists of the coupled evolution of the surface roughness and the surface impurity concentration. The slowly sputtered impurity is randomly distributed in the bulk so that its distribution at the surface is solely determined by the sputtering dynamics. Our $d=1+1$ results show that the long-time scaling exponents are for α approximately 1/2 and β approximately 1/3, for both large and small γ. For the intermediate values of γ probed here, the results for the long-time exponents are less conclusive. However, the roughening behavior is dependent upon the degree of inhomogeneity (tuned by the parameter γ in our calculations). For certain values of γ we find an intermediate-time rapid-roughening regime that persists up to considerable roughness and number of sputtered layers. The range of values for γ for which this happens depends upon the diffusivity of the impurity. The occurrence of this rapid-roughening kinetics is correlated with large fluctuations of the impurity concentration. In this regime, as a consequence of impurity pinning, both scaling exponents α and β gradually increase to values close to 1. The large roughening exponent is consistent with surfaces dominated by conical structures. We find that in this rapid-roughening regime, the slope distribution shows a large peak at a nonzero slope s equal to $(2\mu/\lambda)^{1/2}$; that is, the slope can be tuned by adjusting the flux (through the average velocity μ) and by selecting the material (through λ).

Our results show that the roughening behavior in $d=2+1$ also changes similarly with γ. At zero γ, the kinetics is characterized by an initial rapid-roughening regime, which quickly saturates. The initial regime appears exponential, and the growth exponent for the long-time slow-roughening regime is significantly smaller than the KPZ value as expected. When γ is larger, the roughening behavior is characterized by an initial rapid-roughening regime followed by a slower-roughening regime, both of which show power-law kinetics. The effective growth exponent in the initial regime increases

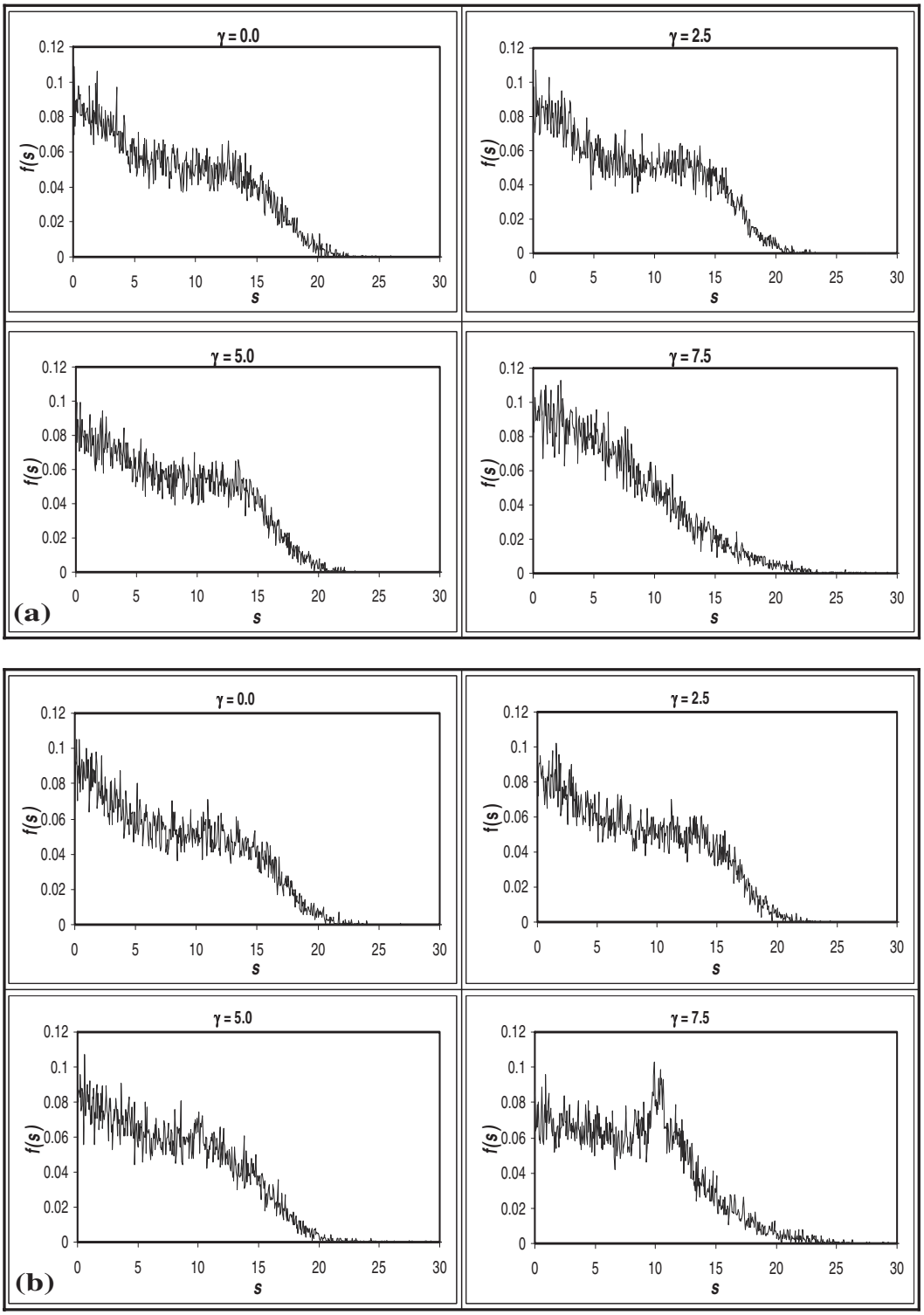

FIG. 12. Plots of the slope distributions for the $\lambda=0.1$ calculations shown in Fig. 9(a). The distributions shown in (a) are at earlier times, the actual number of layers sputtered for each case being about 400. The distributions plotted in (b) correspond to the largest value of roughness in each of the cases shown in Fig. 9(a).

with γ to values close to 1. The largest γ used in our simulations is 15.0, and for this value of γ we obtain a growth exponent of 0.95 for the growth exponent in the initial regime. The longer-time growth exponent also increases with γ, and we obtain a value of 0.39 for γ equal to 15. The surface morphology of the model is significantly noisier than is found for experimental data. In particular, the clear long-range hexagonal (statistical) order that is observed experimentally is not found in our 2+1 simulations, suggesting that a different model than the one investigated here needs to be

considered. However, the roughening kinetics for small γ is similar to the roughening kinetics experimentally observed for GaSb, while the behavior for large γ is similar to experimental results for InP. The long-time roughness reached in our $d=2+1$ simulations is not as large as in our $d=1+1$ simulations. We think much longer simulations with large system sizes are required to provide more definitive data on the growth exponent in the long-time limit. In addition, larger system sizes are probably needed to probe the roughening exponent.

It is known that for the KS equation the initial roughening kinetics can change from a power-law behavior to an apparently exponential behavior in both $d=1+1$ and $d=2+1$ when the stabilizing nonlinear term is relatively small compared to the linear terms. Our simulations show that this exponential behavior can be gradually changed to a power-law scaling by increasing γ (and the inhomogeneity of the surface) while keeping the nonlinear term constant. Thus, depending upon the values of the parameters (principally γ and λ) different roughening kinetics are exhibited by our model.

[1] R. M. Bradley and J. M. E. Harper, J. Vac. Sci. Technol. A **6**, 2390 (1988).
[2] R. Cuerno and A-L. Barabási, Phys. Rev. Lett. **74**, 4746 (1995).
[3] M. Rost and J. Krug, Phys. Rev. Lett. **75**, 3894 (1995).
[4] R. Cuerno, H. A. Makse, S. Tomassone, S. T. Harrington, and H. E. Stanley, Phys. Rev. Lett. **75**, 4464 (1995).
[5] R. Cuerno and K. B. Lauritsen, Phys. Rev. E **52**, 4853 (1995).
[6] K. B. Lauritsen, R. Cuerno, and H. A. Makse, Phys. Rev. E **54**, 3577 (1996).
[7] F. Frost, A. Schindler, and F. Bigl, Phys. Rev. Lett. **85**, 4116 (2000).
[8] S. Facsko, T. Dekorsy, C. Koerdt, C. Trappe, H. Kurz, A. Vogt, and H. L. Hartnagel, Science **285**, 1551 (1999).
[9] E. Chason, T. M. Mayer, and A. Payne, Appl. Phys. Lett. **60**, 2353 (1992).
[10] E. Chason and T. M. Mayer, Appl. Phys. Lett. **62**, 363 (1993).
[11] X. S. Wang, R. J. Pechman, and J. H. Weaver, J. Vac. Sci. Technol. B **13**, 2031 (1995).
[12] X. S. Wang, R. J. Pechman, and J. H. Weaver, Surf. Sci. **364**, L511 (1996).
[13] R. Gago, L. Vásquez, R. Cuerno, M. Varela, C. Ballesteros, and J. M. Albella, Appl. Phys. Lett. **78**, 3316 (2001).
[14] A. C. T. Chan and G. C. Wang, Surf. Sci. **414**, 17 (1998).
[15] D.-M. Smilgies, P. J. Eng, E. Landemark, and M. Nielsen, Europhys. Lett. **38**, 447 (1997).
[16] J. Krim, I. Heyvaert, C. Van Haesendonck, and Y. Bruynseraede, Phys. Rev. Lett. **70**, 57 (1993).
[17] S. G. Mayr, M. Moske, and K. Samwer, Phys. Rev. B **60**, 16950 (1999).
[18] C. Streng, K. Samwer, and S. G. Mayr, Phys. Rev. B **73**, 104107 (2006).
[19] S. W. Ong, E. S. Tok, and H. C. Kang, Phys. Rev. E **70**, 011604 (2004).
[20] T. C. Kim, M. H. Jo, Y. Kim, D. Y. Noh, B. Kahng, and J. S. Kim, Phys. Rev. B **73**, 125425 (2006).
[21] C. Jayaprakash, F. Hayot, and R. Pandit, Phys. Rev. Lett. **71**, 12 (1993).
[22] K. Sneppen, J. Krug, M. H. Jensen, C. Jayaprakash, and T. Bohr, Phys. Rev. A **46**, R7351 (1992).
[23] J. Drotar, Y. P. Zhao, T. M. Lu, and G. C. Wang, Phys. Rev. E **59**, 177 (1999).
[24] T. Bobek, S. Facsko, H. Kurz, T. Dekorsky, M. Xu, and C. Teichert, Phys. Rev. B **68**, 085324 (2003).